Journal of Sound and Vibration (1997) **200**(3), 347–358

ANALYSIS OF THE SOUND GENERATED BY THE PAIRING OF TWO AXISYMMETRIC CO-ROTATING VORTEX RINGS

R. VERZICCO

Università di Roma "La Sapienza", Dipartimento di Meccanica e Aeronautica, via Eudossiana 18, 00184 *Roma, Italia*

A. IAFRATI

C.I.R.A Centro Italiano Ricerche Aerospaziali, via Maiorise, 81043 *Capua* (*CE*), *Italia*

G. RICCARDI

Seconda Università di Napoli, Dipartimento di Ingegneria, via Roma 29, 81031 *Aversa* (*CE*), *Italia*

AND

M. FATICA

Center for Turbulence Research, Stanford University, CA 94305, *U.S.A.*

(*Received* 28 *September* 1995, *and in final form* 8 *August* 1996)

The pairing of two axisymmetric co-rotating vortex rings is considered as a model problem for the interaction of the large scale structures in round jets. By using direct numerical simulations of the incompressible Navier-Stokes equations, the sound radiation of the interaction has been analyzed, with consideration of the effects of the Reynolds number and initial thickness of the rings. The acoustic signature of the interaction has revealed only minor effects of the Reynolds number. But the signature shows large effects of the vorticity distribution, with the eventual appearance of a secondary frequency.

1. INTRODUCTION

The aeroacoustics of round jets is an important technical and environmental problem in particular in aeronautics, where the noise generated by aeroengines has a large relevance. Although there is some controversy about the main cause of noise, Bridges and Hussain [1] have shown that in turbulent jets the noise generated by the dynamics of coherent structures cannot be dominant, while most of the sound radiation is due to the break-up of the jet at the end of the potential core. In contrast, for moderate Reynolds number flows, the main cause of the noise is related to the dynamics of the large vorticity structures arising from the instability of the shear layer immediately outside the nozzle. Experimental visualizations by Yule [2] at low Reynolds number allowed the identification of these structures as vortex rings and he noted that their interaction determined the characteristics of the jet. In particular one of the most relevant acoustic events is the pairing between co-rotating vortex rings and is the main cause of noise.

Powell [3] has shown that, in low Mach number flows and in the absence of solid bodies, the sound source is confined to rotational regions. Möhring [4], introducing a vector Green function, obtained an improved expression for the acoustics, with only vorticity and position vectors being involved. Besides if one is interested only in the far field acoustic

0022–460X/97/080347 + 12 $25.00/0/sv960714

pressure, it can be computed from an *incompressible* calculation by simply taking the third time derivative of the centroid of vorticity as defined by Helmholtz [5]. This result, together with the decoupling of the acoustic pressure from the fluid-dynamic problem [6], provides an important simplification in the acoustic analysis.

In the study presented here, the dynamics of two isolated co-rotating vortex rings have been analyzed with particular attention to the sound generated by their interaction. The aim of this calculation is to isolate the most relevant aeroacoustic phenomenon, on the assumption that the pressure signal is not disturbed by the complex jet dynamics. This simplification might appear too crude, since in a real jet there is an array of vortex rings and not just two. However flow visualizations have shown that these rings always interact in pairs, and therefore the present assumption is appropriate. Besides, due to the easier flow configuration, it is possible to perform a parametric study to understand which factors most influence the noise.

The sound radiated by the mutual threading of two identical co-rotating vortex rings has been previously studied by Kambe and Minota [7] using the hypotheses of inviscid fluid and "thin" rings: i.e., with the core to ring radius ratio $\varepsilon/R \ll 1$. In particular they studied the effect of the initial axial spacing between the rings on the sound radiated. In contrast, in this paper finite core rings in a viscous fluid have been considered with a particular look at the effects of the Reynolds number, the initial vorticity distribution and the core size of the rings. Results have shown that the sound generation is mostly determined by the vorticity distribution inside the ring cores, being more intense for thin cores and sharp vorticity profiles.

Finally, in order to ensure the lack of dependence of the results on the particular computational scheme, and to validate the numerical codes, some of the flows have been simulated by two different procedures. In the first, the equations were solved in the vorticity-streamfunction variables, allowing a direct computation of the acoustic source terms. In the second, primitive variables (velocities and pressure) were used and a preliminary calculation of the vorticity field was necessary. The comparison proved the results to be indistinguishable and this allowed us to perform the analysis without specifying if the results were obtained by the former or the latter numerical approach.

2. ACOUSTIC SOURCE TERMS

Lighthill [6], starting from the Navier-Stokes equations for compressible flows, derived the inhomogeneous wave equation for the density perturbation ϱ,

$$\partial^2\varrho/\partial t^2 + c_0^2\nabla^2\varrho = \partial^2 T_{ij}/\partial x_i \partial x_j, \qquad T_{ij} = \varrho u_i u_j + (p - c_0^2\varrho)\delta_{ij} - e_{ij}, \tag{1}$$

where c_0 is the speed of sound in the undisturbed flow, u_i is the ith velocity component, p is the pressure and e_{ij} is the viscous stress tensor.

For unbounded flows at high Reynolds (Re) and low Mach ($Ma = U/c_0$) numbers, the solution of equation (1) can be decoupled from the fluid dynamic problem. With L and U characteristic velocity and length scales of the flow, the acoustic wavelength is $\lambda = \mathcal{O}(c_0 L/U) = \mathcal{O}(L/Ma)$: i.e., it is much larger than the fluid dynamic length scale L. Since the acoustic perturbation is $\mathcal{O}(Ma^2)$, inside the rotational region it is possible to neglect both acoustic pressure and its variation. In contrast, far from the former region the induced velocity decays as $1/|x|^3$ and the term $\varrho u_i u_j$ becomes second order with respect to the acoustic perturbation. Besides for high Reynolds number flows and with the hypothesis of isentropic flows one has $(p - p_0) \simeq c_0^2(\varrho - \varrho_0)$;

then, far from the rotational region (far field), the source term in equation (1) can be neglected.

Based on these considerations, Kambe [8] analyzed the acoustic pressure induced in the far field by the vorticity dynamics and found the following relation between the vorticity $\boldsymbol{\omega}$ and acoustic pressure:

$$p^*(\mathbf{x}, t) = \frac{1}{12\pi}\frac{\varrho_0}{c_0^2}\frac{1}{|\mathbf{x}|}\left(\frac{x_i x_j}{|\mathbf{x}|^2}\ddot{Q}_{ij}(t_x) + (5-3\gamma)\ddot{K}(t_x)\right). \tag{2}$$

Here γ is the ratio between the specific heats and Q_{ij} and K are defined by

$$Q_{ij}(t) = \int_{R^3} y_i[\mathbf{y}\times\boldsymbol{\omega}(\mathbf{y}, t)]_j \,\mathrm{d}v(y), \qquad K(t) = \tfrac{1}{2}\int_{R^3} |\mathbf{u}(\mathbf{y}, t)|^2 \,\mathrm{d}v(y). \tag{3}$$

$t_x = t - |\mathbf{x}|/c_0$ is the retarded emission time, $\mathbf{x}$ being the distance between the observer and the acoustic source, and the dots over the variables Q_{ij} and K indicate time differentiation.

For axisymmetric flows without swirl the above expressions simplify and the acoustics pressure in a meridional plane A becomes

$$p^*(\mathbf{x}, t) = \frac{1}{4}\frac{\varrho_0}{c_0^2}\frac{1}{|\mathbf{x}|}\left[(\cos^2\phi - \tfrac{1}{3})\ddot{Q}(t_x) + \frac{5-3\gamma}{3}\ddot{K}(t_x)\right],$$

ϕ being the angle between the vector $\mathbf{x}$ and the axis of symmetry. Due to the symmetry, the terms in equations (3) assume the forms

$$Q(t) = \int_A \omega\sigma^2 x \,\mathrm{d}\sigma\,\mathrm{d}x, \qquad K(t) = \int_A \psi\omega \,\mathrm{d}\sigma\,\mathrm{d}x, \tag{4}$$

where σ and x are radial and axial co-ordinates respectively and ψ is the Stokes streamfunction. Because of the characteristics of their directivities the acoustic source terms $\ddot{Q}$ and $\ddot{K}$ are defined as *quadrupole* and *monopole*.

In the following some alternative expressions will also be used for the time-derivatives of K and Q [8]:

$$\begin{aligned}
\dot{K} &= -2\nu\int_A \sigma\omega^2 \,\mathrm{d}\sigma\,\mathrm{d}x,\\
\ddot{K} &= -4\nu\int_A \omega^2 v \,\mathrm{d}x\,\mathrm{d}\sigma + 4\nu^2\int_A\left[\left(\frac{\partial\omega}{\partial x}\right)^2 + \left(\frac{\partial\omega}{\partial\sigma}\right)^2 + \frac{\omega^2}{\sigma^2}\right]\sigma\,\mathrm{d}x\,\mathrm{d}\sigma,\\
\dot{Q} &= \int_A (u\sigma^2 + 2v\sigma x)\omega \,\mathrm{d}\sigma\,\mathrm{d}x.
\end{aligned} \tag{5}$$

It will be seen in the next section that the computation of these derivatives, both directly from equations (5) or by numerical differentiation of equations (4), allows the accuracy of the acoustic results to be checked.

3. NUMERICAL SET-UP

3.1. NUMERICAL SCHEMES

Both numerical methods solve the incompressible Navier-Stokes equations by finite-difference scheme; second-order accurate in space and in time. The first in

vorticity and stream function variables is designed for axisymmetric, swirl-free flows, the equations are:

$$\frac{\partial \omega}{\partial t} + \frac{\partial}{\partial \sigma}\left(\frac{\omega}{\sigma}\right)\frac{\partial \psi}{\partial x} - \frac{\partial}{\partial x}\left(\frac{\omega}{\sigma}\right)\frac{\partial \psi}{\partial \sigma} = \frac{1}{Re}\left[\frac{\partial}{\partial \sigma}\left(\frac{1}{\sigma}\frac{\partial \sigma \omega}{\partial \sigma}\right) + \frac{\partial^2 \omega}{\partial x^2}\right], \tag{6}$$

$$\sigma(\partial/\partial\sigma)(1/\sigma)\partial\psi/\partial\sigma + \partial^2\psi/\partial x^2 = -\sigma\omega, \tag{7}$$

$$u = (1/\sigma)\partial/\partial\sigma, \qquad v = -(1/\sigma)\partial\psi/\partial x, \tag{8}$$

being the axial and radial velocity components, respectively, ψ the Stokes' streamfunction and ω the azimuthal vorticity component. The solution procedure is essentially the same as that of Orlandi and Verzicco [9], the only relevant difference being the solution of the elliptic equation (7) for which the iterative scheme developed by Matrone and Bucchignani [10] is used. At the boundaries of the computational domain the vorticity was set equal to zero while an asymptotic expression for the streamfunction was used to mimic the unbounded space. A fourth order expansion for $\psi = g*\sigma\omega$, with $g(\mathbf{x}) = 1/(4\pi|\mathbf{x}|)$, gives

$$\psi(x,\sigma) \simeq \frac{\sigma^2}{4|\mathbf{x}|^3}\int_A \left\{1 + 3\frac{x}{|\mathbf{x}|^2}x' - \frac{3}{2}\frac{1}{|\mathbf{x}|^2}\left[\left(1 - 5\frac{x^2}{|\mathbf{x}|^2}\right)x'^2 + \left(1 - \frac{5}{4}\frac{\sigma^2}{|\mathbf{x}|^2}\right)\sigma'^2\right]\right.$$

$$\left. - \frac{15}{2}\frac{x}{|\mathbf{x}|^4}\left[\left(1 - \frac{7}{3}\frac{x^2}{|\mathbf{x}|^2}\right)x'^3 + \left(1 - \frac{7}{4}\frac{\sigma^2}{|\mathbf{x}|^2}\right)\sigma'^2 x'\right]\right\}\sigma'^2\omega(x',\sigma')\,\mathrm{d}\sigma'\,\mathrm{d}x'.$$

The second method solves the Navier-Stokes equations in primitive variables. Although this code is capable of solving three-dimensional flows, in this study it has been used in the axisymmetric case. The equations, given by Shariff *et al*. [11] and not reported here for sake of brevity, have been solved by a standard fractional-step method and have been advanced in time by a third order Runge—Kutta scheme. The elliptic equation, necessary to satisfy the incompressibility condition, has been reduced to the inversion of a tridagonal matrix by the introduction of trigonometric expansion in the axial direction. In cylindrical co-ordinates at $\sigma = 0$ the equations for the velocity components are singular, and therefore in the radial direction the equation is solved for the quantity $q_\sigma = \sigma v$. The advantage of staggering the velocities is that at the centerline q_σ is identically zero, and the equation is discretized without any approximation.

Along the axial direction periodicity was assumed, as is usually done in free-shear layers, while a free-slip condition was imposed at the external radial boundary. That the latter boundary was located at a satisfactory distance from the axis, was checked by preliminary simulations.

In both cases the equations have been non-dimensionalized by the circulation of the ring Γ and the toroidal radius of the ring R giving a Reynolds number $Re = \Gamma/\nu$ with ν the kinematic viscosity. The equations have been solved in a region of axial and radial lengths respectively of $10R$ and $4R$.

For the numerical calculation of the integrals (4) and (5), standard second-order and generalized fourth-order Simpson rules [12] have been used, giving practically the same results. Also, for the calculation of the numerical time derivatives of K and Q second and fourth order accurate expressions have been employed, again giving the same results.

3.2. INITIAL CONDITIONS

Most of the simulations have been performed with the initial condition assumption of two identical vortex rings initially at a distance equal to their toroidal radius R and with Gaussian vorticity distribution within the core,

$$\omega(x, \sigma) = (\Gamma/\pi\varepsilon^2)\, \mathrm{e}^{-(s/\varepsilon)^2}, \qquad \text{with} \qquad s^2 \equiv (x - X_0)^2 + (\sigma - R)^2, \tag{9}$$

where $X_0 = \pm R/2$ for the first and second rings, respectively. ε is the radius of the core, and s is the radius of the polar co-ordinates centred at the core (see Figure 1). From equation (9) it is possible to derive the expression for the velocity tangential to the core,

$$u_\varphi = (\Gamma/2\pi s)[1 - \mathrm{e}^{-(s/\varepsilon)^2}] \tag{10}$$

that will be found to be useful later.

In order to investigate about the role of the core vorticity distribution on the sound generated, a second set of simulations has been performed with a further initial condition of having a "top-hat" vorticity in the core,

$$\omega(x, \sigma) = \mathscr{C}\sigma \begin{cases} 1 & s \leqslant 0{\cdot}8\varepsilon \\ 1 - f(\eta) & 0{\cdot}8\varepsilon < s < 1{\cdot}2\varepsilon \\ 0 & 1{\cdot}2\varepsilon \leqslant s \end{cases}, \tag{11}$$

where $f(\eta) = \exp[-\mathrm{e}^2(\log 2/2)(1/\eta)\exp(1/(\eta - 1))]$ and $\eta = (s - 0{\cdot}8\varepsilon)/(0{\cdot}4\varepsilon)$. The function f is introduced to smooth the vorticity discontinuity between the core of the ring and the external irrotational region. The constant $\mathscr{C}$ is fixed by the requirement of a vortex ring with unit circulation.

As mentioned above, the initial spacing between the rings has been assumed, for all the simulations, to be equal to the ring radius R. Indeed, in a parametric study of the vortex ring pairing, the effect of the initial axial distance, could also be considered. However, by increasing the initial spacing of the rings the passage interaction is delayed without evident changes in the dynamics. On the other hand, for every large initial distances, due to viscous effects, interaction occurs when the vortices are very weak and the problem becomes irrelevant for the jet. Actually, upon considering that the fundamental frequency of shear-layers is $St_\theta = f\theta/U = 0{\cdot}012$–$0{\cdot}013$ (with U the centerline jet velocity, θ the momentum thickness of the shear-layer and f the frequency), it turns out that the round jet generating the present initial flow configuration should have $R/\theta \simeq 40$, which is a realistic value for jets. Indeed, the instability organizing the vorticity into rings is a second

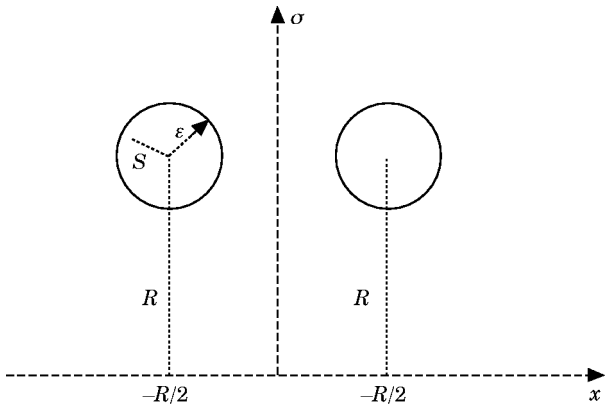

Figure 1. Sketch of the initial conditions.

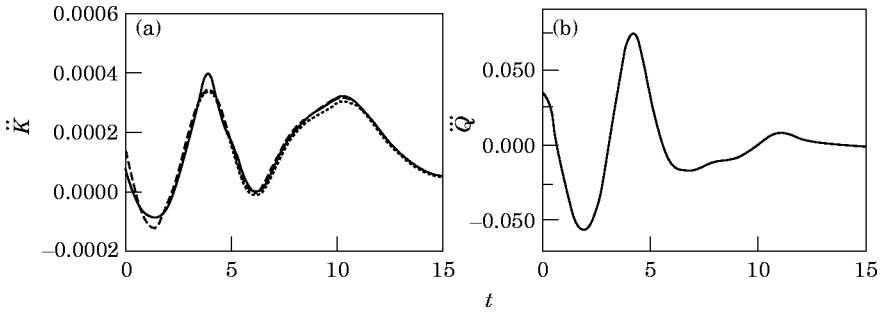

Figure 2. Time evolution of the acoustic terms for the interaction of two co-rotating vortex rings with Gaussian initial vorticity distribution ($\varepsilon/R = 0{\cdot}3$) and $Re = 2500$. (a) Monopole term; ——, second derivative of K; - - - -, first derivative of $\dot{K}$; · · · ·, $\ddot{K}$. (b) Quadrupole term; ——, third time derivative of Q; - - - -, second derivative of $\dot{Q}$.

instability called the preferred mode [1], whose frequency scales with the jet diameter $D \simeq 2R$ and its value is $St_D \simeq 0{\cdot}5$. Although this value yields an axial spacing of the vortex ring of about $D \simeq 2R$ this instability is quite broadband and many flow visualizations (see, for example, the paper by Suprayan and Fiedler [13]) have shown vortex ring at an axial distance of R which is the value presently used.

3.3. CONVERGENCE CHECKS

The spatial resolution of the simulations was fixed such that the acoustic terms could be accurately computed and were independent of the mesh size. Successive grid refinements revealed that a grid spacing $\Delta \simeq R/50$ in the radial and axial directions was enough for the present purposes at $Re = 2500$.

In particular for the quadrupole term the second numerical derivative of $\dot{Q}$ given in the last of equations (5) with the third numerical derivative of Q has been computed, while for the monopole term the second derivative of K has been compared with the first derivative of $\dot{K}$ and $\ddot{K}$ directly computed from the second of equations (5).

Preliminary tests have shown that the monopole term is the most sensitive to the spatial resolution and coarse grids are immediately evidenced by large discrepancies between the computed $\ddot{K}$. In Figure 2 is shown the comparison for an adequately resolved case.

A few words should be said about the non-dimensionalization of the acoustic source terms. Kambe and Minota [7] presented their results normalized with the quantity ΓU_0^3, where $U_0 = \Gamma/4\pi R$. In the present case, however, all rings have unit circulation and unit toroidal radius, and therefore such scaling would result in a division of all results by a constant factor. Another possibility is the choice made by Shariff *et al*. [14] who normalized the results with the same quantity but with U_0 being the speed of translation of the steady vortex ring in isolation, $U_0 = \Gamma/4\pi R[\ln(8R/\varepsilon) - 1/4]$. This latter choice introduces a dependence of the scaling factor on the core thickness of the ring. Actually, since thin core rings move faster, thus producing higher levels of noise, this scaling might eliminate the dependence of the acoustic source terms on the core size. This non-dimensionalization has been tested on the present results; however, the physical behaviour of the quadrupole and monopole terms was observed to be the same as their dimensional counterparts, and thus it is preferable to present the results without any scaling.

4. RESULTS

Before getting into the discussion of the acoustics, it is useful to describe the vorticity dynamics that characterizes the sound radiation through equation (4). In

Figure 3(a) is shown the initial configuration, that consists of two identical vortex rings with Gaussian vorticity distribution, with the ratio core-to-ring radius $\varepsilon/R = 0{\cdot}3$. Both rings, due to the self-induced translation velocity move in the same direction (from right to left in Figure 3) and of course if they were isolated they would have an identical translation velocity. In this flow configuration however, the rear one is compressed toward the axis of symmetry, and the increasing curvature increase also its translation velocity. This leads to rear ring to overtake the first ring, passing through the inner region. On the other hand while the rear ring is passing through, the other ring is pushed radially outward so that its toroidal radius increases and the velocity decreases, and this further helps the overtaking phenomenon. It might happen that when the first passage is completed there is a second interaction that eventually could restore the initial configuration, and the process can continue. This is a classical model of rings interaction called "leapfrogging"; that, however, requires an "elastic" interaction between the rings with no permanent deformations of the cores. Shariff *et al*. [15], by contour-dynamics calculations, have shown that this scenario is unlikely even if viscosity is cancelled out. In particular the rings, during the interaction, tear each other and pair (but not merge) forming a large structure with sparse filaments. They also showed that the classical picture holds only for extremely thin cores that cannot be found in real jets. In the present case the first interaction is accompanied by strong core deformations, the rear ring wraps around the first and the viscosity merges the two structures into only one ring, with only a weak tail left behind (see Figure 3(f)). This is the kind of interaction commonly observed in jets where large vortical structures tear each other and finally pair.

It is worth noting that the pairing of axisymmetric vortex rings is quite different from that in two dimensions. In the latter case in fact, the vortices come closer, co-rotate and pair by maintaining a perfect symmetry. In contrast, during the pairing of vortex rings one is strained below the other and, due to vortex-stretching, vorticity levels change considerably inside the rings. Shariff *et al*. [14] pointed out that the asymmetry of the interaction is due to the unequal strain rate histories experienced by the vortices. This last argument partially explains the experimental observation of Hussain [16] who noted that, differently from plane mixing-layers, in round jets the evolution of large-scale structures primarily occurs through asymmetric and fractional pairings.

The acoustic signals generated by the interaction of the two rings is shown in Figure 4 and, to relate better vorticity dynamics and acoustics, solid symbols in Figure 4(a) indicate the times of the frames of Figure 3. Both contributions behave as a damped oscillation,

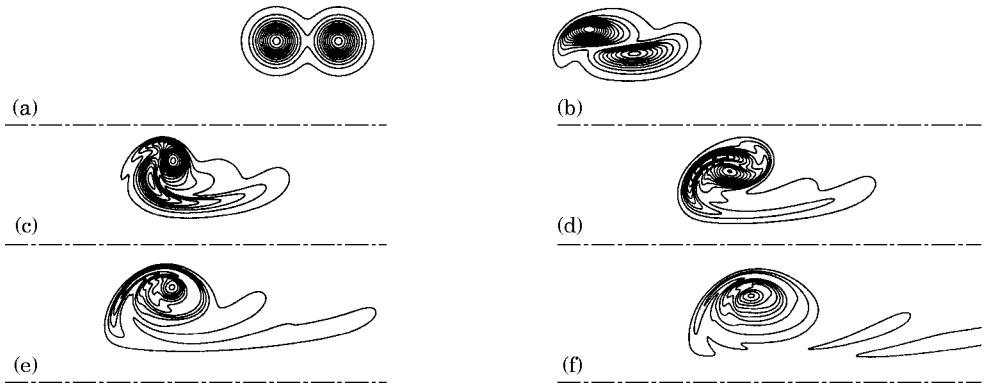

Figure 3. Contour plots of azimuthal vorticity for the interaction of two co-rotating rings with Gaussian vorticity distribution ($\varepsilon/R = 0{\cdot}3$) at $Re = 2500$. (a) $t = 0$; (b) $t = 2$; (c) $t = 4$; (d) $t = 6$; (e) $t = 10$; (f) $t = 14$. The line – - – indicates the axis of symmetry, $\Delta\omega = 0{\cdot}3$. Rings move from right to left.

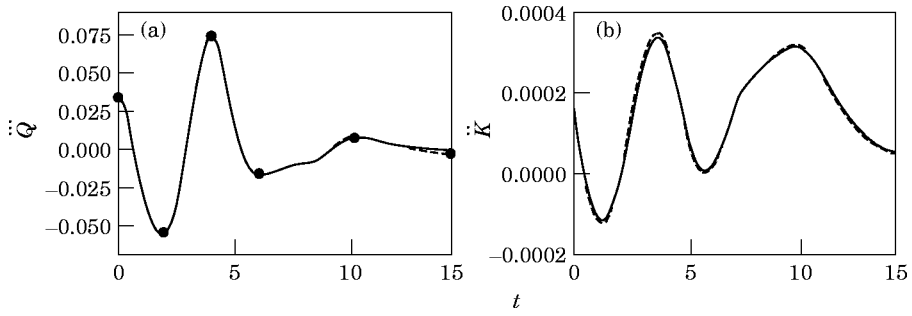

Figure 4. Time evolution of the acoustic source terms for the case of Figure 2. (a) Quadrupole, (b) monopole term. ——, Vorticity stream function formulation; – – –, primitive variables. Symbols ● indicate the times of the frames of Figure 2.

with a characteristic frequency which is that of the passage of one ring inside the other, and a damping that depends on how fast the rings merge. It will be shown in what follows that the latter factor is influenced by the Reynolds number and by the vorticity distribution inside the core of the vortex; in the present case for $t \geqslant 10$ the pairing of the rings is completed, the vorticity is adjusted in one large structure and the acoustic pressure quickly vanishes. It can also be noted that the quadrupole term is about one order of magnitude larger than the monopole and since in equation (2) $\ddot{Q}$ is the only term having a spatial dependence, the acoustic radiation has a marked quadrupolar character.

As a consistency check for the numerics, the same flow has been simulated by the code in vorticity-streamfunction and by that in primitive variables. The result is shown in Figure 4 and the comparison looks very satisfactory.

The influence of viscous effects on the acoustic emission has been investigated by performing the previous simulation for a higher and lower value of the Reynolds number. The vorticity dynamics presents only minor differences, and therefore the fields are not reported, while the acoustic terms are shown in Figure 5. The quadrupole is essentially unchanged due to the fact that the "leapfrogging" of one ring inside the other is an inviscid phenomenon; however it is evidently the effect of viscosity that smooths vorticity gradients and slightly slackens the dynamics. Both these effects diminish the magnitude of the quadrupole. In contrast, the monopole results are largely affected by the viscosity, and in particular this grows as the Reynolds number decreases. This is easily understood since the amplitude of the monopole term depends on how fast the kinetic energy is dissipated and obviously the lower the Reynolds number the faster the energy decreases. In all cases,

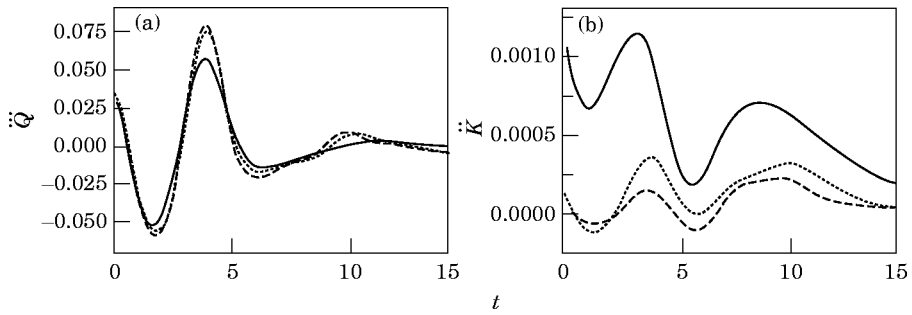

Figure 5. Time evolution of the acoustic terms for the interaction of two co-rotating rings with Gaussian vorticity distribution ($\varepsilon/R = 0{\cdot}3$): ——, $Re = 1000$: · · · ·, $Re = 2500$; - - -, $Re = 4000$. (a) Quadrupole, (b) monopole term.

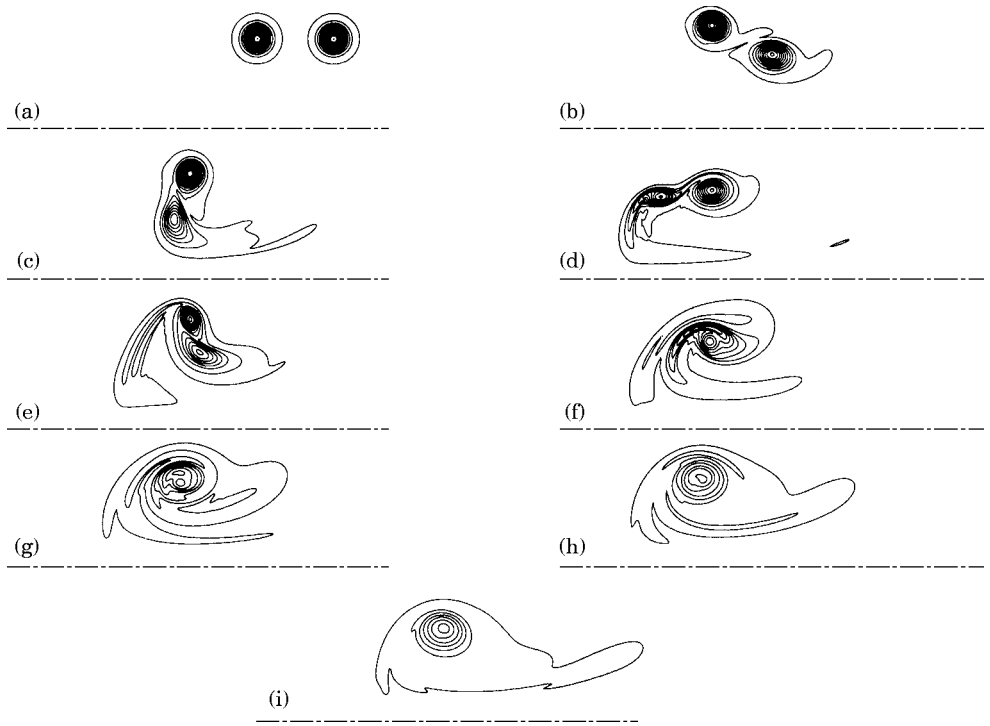

Figure 6. Contour plots of azimuthal vorticity for the interaction of two co-rotating rings with Gaussian vorticity distribution ($\varepsilon/R = 0{\cdot}15$) at $Re = 2500$. (a) $t = 0$; (b) $t = 2$; (c) $t = 4$; (d) $t = 6$; (e) $t = 8$; (f) $t = 10$; (g) $t = 12$; (h) $t = 14$; (i) $t = 16$. The line — · — indicates the axis of symmetry, $\Delta\omega = 1$. Rings move from right to left.

however, after the pairing is completed and only one structure is formed both terms drop to zero and maintain this value for the rest of the evolution.

A major factor influencing the acoustic radiation is the thickness of the ring given by the ratio of the core to toroidal radius ε/R. In order to investigate this effect simulations have been performed with the same parameters as the case of Figure 3 but using thinner and thicker rings. The case with thicker rings ($\varepsilon/R = 0{\cdot}4$) does not present any particular feature; the vorticity dynamics is the same as in the previous case but, since the self-induced translation velocity is smaller and "fat" rings interact in a slower manner, the acoustic radiation is considerably lower (see Figure 7). On the contrary the dynamics becomes much more active for the case of thinner rings ($\varepsilon/R = 0{\cdot}15$), and some flow maps are shown in

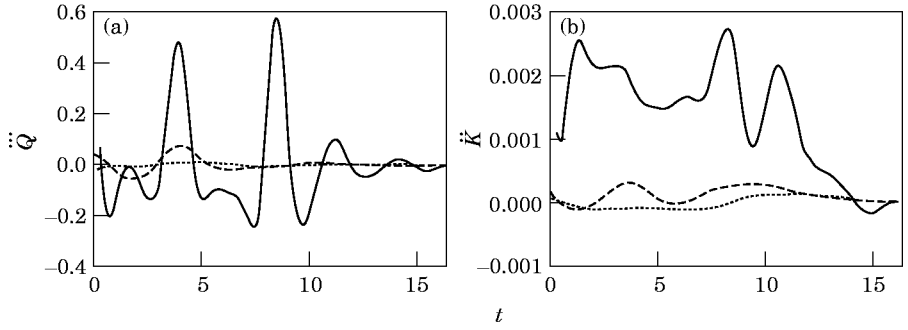

Figure 7. Time evolution of the acoustic source terms for the interaction of two co-rotating rings with Gaussian vorticity distribution at $Re = 2500$: ——, $\varepsilon/R = 0{\cdot}15$; - - -, $\varepsilon/R = 0{\cdot}30$; · · · ·, $\varepsilon/R = 0{\cdot}40$; (a) Quadrupole term, (b) monopole term.

Figure 6. A first effect is that, since the cores are small, the scenario of the interaction is closer to the classical "leapfrogging" and after the first passage ($t = 6$) the pairing is not completed. In particular at $t \simeq 8$ there is a second passage accompanied by large deformations of the ring cores that are also evidenced by the peak in the quadrupole term of Figure 7(a). A new feature that appears in both monopole and quadrupole terms is a secondary frequency higher than that of the passage. This frequency is due to the nutation of the ring cores and its related period is the eddy-turnover-time of the single rings. In fact, defining the eddy-turnover-time as the time it takes a particle to revolve around the core at a location $s = \delta$ of maximum tangential velocity in the core (u_φ), one has from equation (10) $\delta = 1{\cdot}12141\varepsilon$ and $u_\varphi(\delta) = 0{\cdot}1139\Gamma/\delta$. Finally the eddy-turnover-time T is

$$T = 2\pi\delta/u_\varphi(\delta) = 2\pi\delta^2/0{\cdot}1139\Gamma,$$

so that for $\varepsilon = 0{\cdot}15$ and $\Gamma = 1$ one has $T = 1{\cdot}560$. This is exactly the period of the first oscillation in the quadrupole term and this frequency is also evident later, even if it is partially hidden by the large amplitude of the low frequency component.

The amplitudes of the monopole, given in Figure 7(b), show that it increases as the rings become thinner and this is consistent with the energetic meaning of the monopole as a rate of dissipation. In fact when the core radius decreases the gradients become steeper and steep gradients are always accompanied by a large dissipation (see equation (5)).

The fundamental importance played by vorticity gradients in the acoustic radiation is confirmed also by the simulation performed with the rings given by equation (11) with a "top hat" initial vorticity distribution. In this case the vortex rings are as thick as in the first case ($\varepsilon/R = 0{\cdot}30$) but high vorticity gradients are introduced by the different vorticity distribution. Results are reported in Figure 8, showing that again high vorticity gradients increase the magnitude of both monopole and quadrupole terms, even if different from the thin core case there is no evidence of the secondary frequency. This is due to the nutation of the ring, which for the present core-thickness is much slower. In fact, assuming as rough estimate of the eddy turnover-time the value for the corresponding Gaussian ring with $\varepsilon/R = 0{\cdot}30$, one obtains $T \simeq 6{\cdot}3$, yielding a secondary frequency lower than the fundamental one. Since the magnitude of the quadrupole term is given by the third time derivative of Q, it is clear that the slower the time scale of the phenomenon, the more the amplitude will be reduced.

In order to separate the effect of viscosity from that of convection, a similar simulation has been performed by a contour-dynamics approach [14]. This algorithm describes the inviscid dynamics of a piecewise constant ω/σ region in a Lagrangian manner, following its contour motion. In this context the vorticity distribution given by equation (11), with

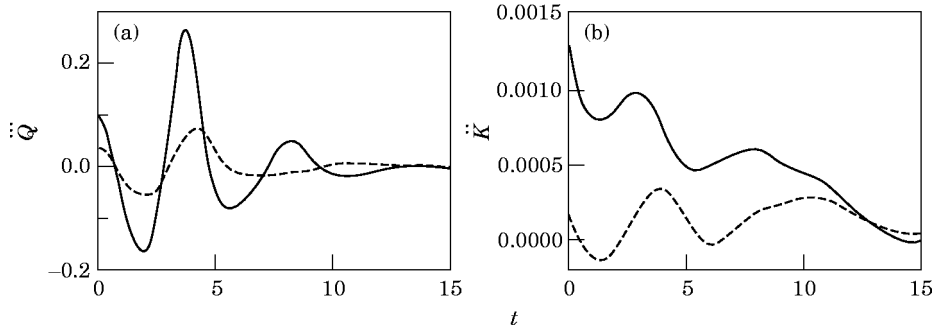

Figure 8. Time evolution of the acoustic terms generated by the interaction of two vortex ring with $\varepsilon/R = 0{\cdot}3$ and $Re = 2500$: —— "top hat", – – – Gaussian vorticity distribution. (a) Quadrupole term, (b) monopole term.

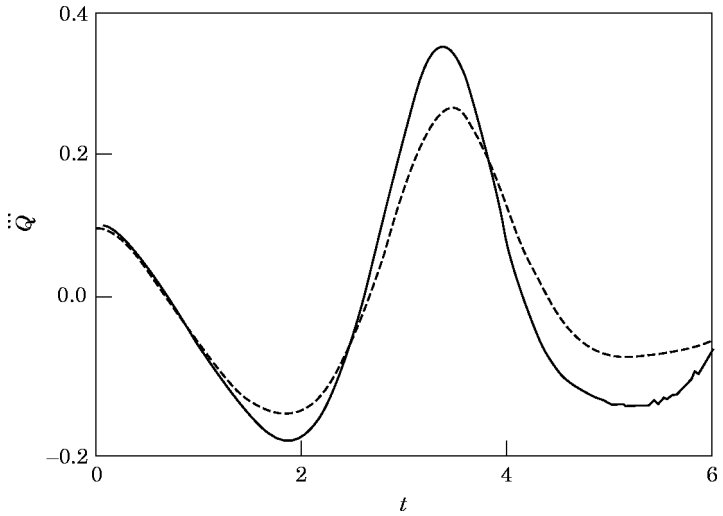

Figure 9. Time evolution of the quadrupole term generated by the interaction of two vortex ring with $\varepsilon/R = 0{\cdot}3$: —— "top hat" contour dynamics; – – – "top hat" with smoothing and $Re = 2500$.

the smoothing function $f(\eta)$ cancelled out, has been used as initial condition. The comparison with the finite-difference solution shows (see Figure 9) that, at least during the passage phase, sound radiation is mostly dominated by the convective terms, giving an acoustic signature very similar to that of the viscous calculation. In particular the frequency of oscillation remains essentially unchanged, while the peak values are slightly smoothed, presumably due to viscous diffusion.

Incidentally, it must be stressed that the interaction between co-rotating vortex rings is accompanied by some filamentation that, in absence of viscosity, generates extremely thin structures which are very difficult to follow by contour-dynamics techniques. This is the reason that the authors were forced to stop the calculation just after the completion of the first passage.

From the above results one can conclude that the acoustic source terms always contain one fundamental frequency related to the passage of one ring inside the other and a secondary frequency due to the nutation of the vortex ring cores. The relative magnitude of the two contributions is usually different and that at the fundamental frequency is the most important contribution. Nevertheless, Shariff *et al*. [15] have shown that there are some extreme cases with inviscid and extremely thin vortex rings where the two contributions have comparable magnitudes and the sound is dominated by the secondary frequency. These cases, however, have mostly a theoretical interest, since such extreme conditions are never encountered in the real jets to which attention was devoted in this study.

5. CONCLUSIONS

Numerical experiments of the interaction between two identical co-rotating vortex rings have been presented with particular consideration of the sound radiation. Simulations performed with different values of the Reynolds number revealed that when viscosity is increased, the quadrupole term decreases while the monopole term increases. However, since the former term has a much larger amplitude, the overall effect is a decrease of the radiated power. On the other hand, when high vorticity gradients are introduced, either by considering thin core rings or sharp initial vorticity distributions, both monopole and

quadrupole terms increase and this latter factor is much more effective than the Reynolds number.

Results have also shown that sound is radiated at two frequencies: a fundamental one, due to the passage of one ring inside the other, and a secondary one with a period equal to the eddy turnover-time of the ring. The former usually constitutes the largest contribution to the sound, while the latter becomes appreciable only when very thin cores are considered. However there might be extreme cases where the secondary frequency becomes the most important [15], even if it happens when zero viscosity and unrealistically thin rings are considered.

ACKNOWLEDGMENTS

Three of us, R.V., G.R. and M.F. acknowledge C.I.R.A. (Centro Italiano Ricerche Aerospaziali) for supporting this research. We are grateful to Dr. K. Shariff for helpful discussions and for his patient work of correction of the manuscript. We wish to thank Prof. G. M. Lilley for a careful reading of the manuscript before submission.

REFERENCES

1. J. E. Bridges and A. K. M. F. Hussain 1987 *Journal of Sound and Vibration* **117**, 289–311. Roles of initial condition and vortex pairing in jet noise.
2. A. J. Yule 1978 *Journal of Fluid Mechanics* **89**, 413–432. Large–scale structure in the mixing layer of a round jet.
3. A. Powell 1964 *Journal of Acoustical Society of America* **36**, 177–195. Theory of vortex sound.
4. W. Möhring 1978 *Journal of Fluid Mechanics* **85**, 685–691. On vortex sound at low Mach number.
5. H. Helmholtz 1858 *Philosophical Magazine Journal of Science* **33**, 485–512. On integrals of the hydrodynamical equations which express vortex motion.
6. M. J. Lighthill 1952 *Proceedings of the Royal Society* **A211**, 564–587. On sound generated aerodynamically. I. General theory.
7. T. Kambe and T. Minota 1981 *Journal of Sound and Vibration* **74**, 61–72. Sound radiation from vortex systems.
8. T. Kambe 1984 *Journal of Sound and Vibration* **95**, 351–360. Influence of viscosity on aerodynamic sound emission in free space.
9. P. Orlandi and R. Verzicco 1993 *Journal of Fluid Mechanics* **256**, 615–646. Vortex rings impinging on walls: axisymmetric and three-dimensional simulations.
10. A. Matrone and E. Bucchignani 1994 *CIRA TR*-94-0088. FLISYS package—User Guide.
11. K. Shariff, R. Verzicco and P. Orlandi 1994 *Journal of Fluid Mechanics* **279**, 351–375. A numerical study of three-dimensional vortex ring instabilities: viscous correction and early non-linear stage.
12. W. H. Press, S. A. Teukolsky, W. T. Vellering and B. P. Flannery 1992 *Numerical Recipes*. Cambridge University Press.
13. R. Suprayan and H. E. Fiedler 1994 *Meccanica* **29**, 403–410. On streamwise vortical structures in the near-field of axisymmetric shear layers.
14. K. Shariff, A. Leonard and J. H. Ferziger 1989 *NASA TM*-102257. Dynamics of a class of vortex rings.
15. K. Shariff, A. Leonard and J. H. Ferziger 1988 *Fluid Dynamics Research* **3**, 337–343. Acoustics and dynamics of coaxial interacting vortex rings.
16. A. K. M. F. Hussain 1980 *Lecture Notes in Physics* **136**, 252–291. Coherent structures and studies of perturbed and unperturbed jets.